ELSEVIER

Journal of Nuclear Materials 255 (1998) 174–179

journal of nuclear materials

Texture and residual-stresses analysis in Zircaloy-4 cylindrical samples

R. Guillen *, C. Cossu, M. François, E. Girard

Laboratoire d'Applications des Matériaux à la Mécanique, IUT Saint-Nazaire, CRTT, Bd de l'Université, BP 406, Saint-Nazaire cedex 44602, France

Received 31 October 1997; accepted 27 January 1998

Abstract

Texture and residual-stress analysis using X-ray diffraction have been carried out on cylindrical Zircaloy-4 samples in cold-worked and finished state. The (00.2) pole figure of finished tubes shows an important asymmetry in the tangential direction (TD) not observed on unrolled tubes. This asymmetry vanishes at a 5-μm depth. A noticeable variation of the texture index J has been pointed out within the first micrometers from the surface of the tubes. Strain measurements in tangential and longitudinal directions have been carried out on the (10.4) and (20.2) planes. In the tangential (hoop) direction, compressive stress on the outer surface decreases rapidly in the first layers and remains constant at the analysed depth. Axial stress analysis shows the opposite sign for the two different diffracting planes on the cold-worked tubes, indicating the existence of second-order stresses.

1. Introduction

The crystallographic texture of a specimen associated with the anisotropy of its crystalline properties can induce a strong anisotropy of its macroscopic properties. This is the case, for instance, with Zircaloy-4 (ZY4), a hexagonal zirconium-based alloy widely used for cladding tubes of nuclear combustibles in pressurised water reactors. This alloy has a very good mechanical behaviour, a very high resistance to corrosion, a good thermal conductivity and a low neutron cross-section.

The ZY4 cladding tubes are manufactured by cold rolling. To arrive at its final size (9.5-mm diameter, 0.6-mm thickness), the material undergoes five cold-rolling passes in a particular mode called cold pilgering. After the four first passes, it is thermally recrystallised and, after the fifth one, it can undergo either a stress-relief heat treatment or a recrystallisation process.

The ZY4 tube crystalline texture induced by this thermo-mechanical process, has been widely analysed [1–7]. In X-ray diffraction (XRD) analysis, the (00.2) pole figure (PF) shows a bimodal distribution of intensities in the ND–TD plane (ND: normal direction, TD: tangential direction). As was previously shown [2], the c/a ratio of ZY4 and the deformation path together lead to this bimodal texture. More precisely, the Q_p factor, ratio between the thickness reduction and the tube diameter reduction, has an important influence on the texture of the tube. The tubes reduced mainly in thickness and a bit in their diameter will be more compressed in radial direction than in tangential direction. In this case, the basal planes will tend to have a radial orientation because they follow the real direction of the compressive force. During the manufacturing process, the texture vary from a tangential trend, for the initial material, to a radial trend, for the final one, all this in accordance with the mechanical reduction coefficients used for pilgering [6]. In the final state, the (00.2) pole figure exhibits intensity maxima in the NT–TD plane at about 30° of the ND axis. The recrystallisation process leads to a noticeable decrease of the bimodal disposition of the intensity maxima in the ND–TD plane with a 30° reorientation of the c axis towards the rolling (axial) direction (RD), this new arrangement of the crystallites can be noticed on (10.0) and (11.0) pole figures. An eventual

* Corresponding author. Tel.: +33-2 40 17 26 25; e-mail: guillen@iutsn.univ-nantes.fr.

0022-3115/98/$19.00
PII: S0022-3115(98)00020-8

stress relief heat treatment, applied in the final manufacturing phase, does not seem to affect the crystalline texture obtained by cold rolling.

Nevertheless, tubes crystalline texture studies realised up to now have been realised on samples unrolled and made thinner chemically with a solution of HF and HNO_3 up to a maximal thickness of 100 μm in order to obtain a plane sample. In the present work, non-unrolled cylindrical samples are studied in order to check previous results and to detect potential skin effects.

A methodology used to perform XRD texture analysis on cylindrical samples has been presented in another paper [8]. The study of samples having a curved geometry (like a small diameter cylinder) not only requires an accurate positioning of the samples but also to take into account the geometric effects induced by the XRD directional feature. We have solved both problems simultaneously by developing a model to describe the diffraction phenomenon with a ray tracing method. Correction coefficients accounting for the 'geometrical texture' of the sample as well as absorption corrections are calculated. The obtained results are used to correct experimental pole figures.

We have developed an experimental device allowing to achieve XRD experiments on such cylindrical samples [9]. This kappa goniometric device has the useful freedom for a good positioning of the diffraction set and it allows texture and residual-stress analysis of important volume and weight samples.

In this work, we analysed the texture of ZY4 tube in two states: directly after fifth pass cold work (CW) or after a subsequent heat treatment and finishing (F) stage in order to compare these results to those obtained on plane samples.

On unrolled samples after the final pass, no noticeable difference in texture can be detected between the two tubes. We realised the same study on the corresponding cylindrical samples so as to point out possible skin effects. With the aim of confirm those results, we achieved a study allowing to detect a possible texture gradient in the thickness of the tube. Besides, residual-stress analysis have been achieved so as to check up an eventual correlation between the mechanical state and the microstructure of the surface.

2. Experimental

The ZY4 tubes have been obtained after five rolling passes by cold-pilgering process. Their dimensions after forming are: 9.5 mm external diameter, 0.6 mm thickness. For the analysis in the tube depth, layers of various thickness were removed by chemical etching. The set of the studied samples is presented in Table 1.

XRD texture analysis has been performed with a four circles kappa goniometer built in our laboratory [9]. The K_α copper radiation has been used. The X-ray beam output collimator had 0.5 mm diameter. To record diffraction peaks, an Inel Position Sensitive Detector (PSD) was used. The coordinates transformation formulae for using a PSD in back reflection proposed by Wcislak and Bunge [10] were applied. We realised incomplete PF with tilt angle varying from 0° to 75° by step of 5°, the azimuthal angle varied from 0° to 360° by step of 5°. For each experimental direction a diffraction pattern with two or three peaks is adjusted, using a nonlinear least squares analysis and assuming pseudo-Voigt peak profiles for each peak, to evaluate background noise and to obtain peak intensities.

As was demonstrated in another work, for XRD texture experiments on cylindrical samples [8], a $G(\psi,\phi)$ factor must be taken into account to correct diffracted intensities from geometrical effects. A ray tracing method has been used with a number of rays in the beam higher than 10 000. This factor is

$$G(\psi,\phi) = \frac{1}{\sum m} \sum_{j=i}^{N_{rays}} \frac{\cos\omega_i(j)}{\frac{1}{\cos\omega_i(j)} + \frac{1}{\cos\omega_d(j)}}, \qquad (1)$$

where ω_i and ω_d are the angles between the normal to a surface element dS and the incident and diffracted rays respectively. ω_i and ω_d depend on ψ and ϕ values. $\sum m$ is a normalisation coefficient. From this result, it can be

Table 1
Identification of ZY4 samples studied indicating removed thickness

State		Removed thickness (μm)
Fifth pass cold worked ZY4 tube	Finished ZY4 tube	
CW0	F0	0
CW5	F5	5
CW10	F10	10
CW20	F20	20
	F41	41
CW43		43
CW200	F200	199

CW: Cold Worked tube, F: Finished tube.

seen that the factor $G(\omega,\phi)$ depends on the orientation of each element of surface and therefore on its geometry. Moreover, the incident ray is diffracted only if the angle ω_d is below $\pi/2$, so for each ray, we calculate a coefficient after having checked that $\cos\omega_d > 0$.

The even part of the orientation distribution function (ODF) calculation has been performed with experimental PF (00.2), (10.1), (11.0) and (10.3) corrected with geometric factors. The series expansion method was used with maximal rating development $L_{max} = 16$. Strain measurements for residual-stress analysis have been carried out on a D500 Siemens goniometer with a K_α chromium radiation. A slit system limits equatorial divergence and back Soller slits limit axial divergence. A Ω goniometric assembly and a SiLi semiconductor detector were used. Tangential (hoop) and axial measurements were achieved on tubes for (10.4) family planes at 156.7° (2θ) and only axial measurements were made for (20.2) planes at 137.2° (2θ) because, due to the texture, the intensity in the tangential direction was too weak. ψ angles varied from $-48°$ to 45°. For tangential analysis, tubes have been placed vertically on a motorised device to allow its continuous rotation, in this way, the analysed volume is statistically more representative. The stress was obtained, using macroscopic elasticity constants, through a refinement scheme similar to a Rietveld structure refinement [11]. However, the refined parameter is the stress instead of the lattice spacing. Thus, the set of diffraction peaks obtained for all the tilt angles are fitted simultaneously with a Pearson VII or a Pearson IV functions, the centroid of all the peaks being related by the $\sin^2\psi$ relation. In spite of the strong texture of the samples, the $\sin^2\psi$ model remains valid because zirconium and ZY4 crystal is close to the elastic isotropy. This is validated by a R^2 confidence factor which shows that experimental data follows the $\sin^2\psi$ relation within the fluctuations due to counting statistics.

3. Results and discussion

3.1. Texture analysis

The first study has consisted in establishing if the cold-worked (CW) tube texture is the same than the finished tube texture, as is the case for unrolled ZY4 samples [6]. A first visual comparison can be achieved studying the pole figures of the (00.2) plane for the samples CW0 and F0 (without any layer removal). The CW sample presents a symmetric PF (Fig. 1a) with a bimodal distribution of the intensity maxima which is typical for this type of sample, in accordance with the results obtained on unrolled samples. It can be noticed in Fig. 1b that finished tubes present an important asymmetry in the ND–TD plane. This asymmetry could not be pointed out on unrolled samples. Two questions are asked in front of this result: (1) what is the cause of the noticed asymmetry and (2) why has not it been detected in unrolled samples.

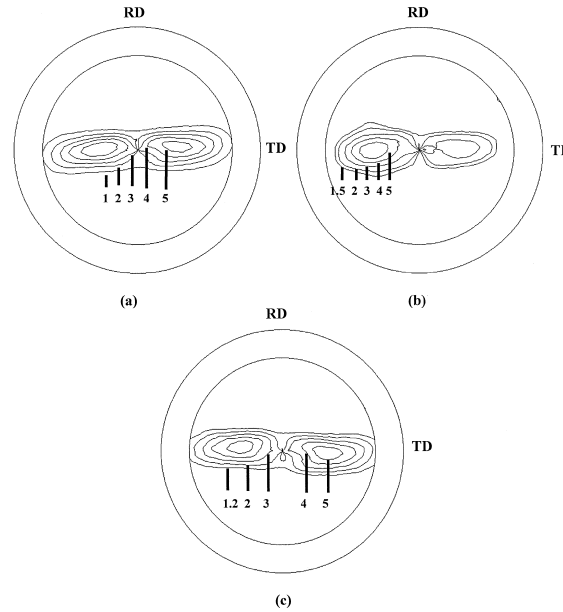

Fig. 1. Experimental (00.2) incomplete PF of cylindrical Zircaloy-4 samples showing surface effects: (a) fifth pass cold worked CW0, (b) finished tube F0 and (c) finished tube 5 μm surface removed F5.

Concerning the first question, it is important to know what happens to the tube after the third cold-rolling pass. It undergoes a stress relief heat treatment which does not induce noticeable change of the crystallites orientation. After this thermal processing, the tube runs through the finishing stages. The texture analysis performed after each finishing stage has shown that the last stage, which is a in line mechanical burnishing, is responsible for the noticed difference. It is well established that this mechanical treatment can lead to important variations of the surface state of the sample, these variations depend on many parameters linked to the burnishing conditions: its nature, the type of the surfaces in contact, its direction, the duration, etc.

Concerning the second question, to observe the external surface in unrolled samples, the tube was chemically thinned from the inside after having protected the external surface. Nevertheless, it is likely that weak thickness (a few micrometers) of the external surface are affected by the chemical attack. A texture analysis in the tube thickness confirms this hypothesis, because for the F5 sample (5 μm removed finished tube) we point out (Fig. 1c) a distribution of the poles densities which is similar to the distribution obtained for the CW tube. The PF of more removed samples confirm the lack of asymmetry and the likeness with the PF of CW0 sample.

It seems important to confirm these results by analysing the penetration depth of X-rays in the samples. Taking into

account the energy of the used radiation and the nature of the material, it is easy to calculate the proportion of the diffracted radiation associated to a given depth using the well-known equation $I = I_0 e^{-\mu x}$, where I is the intensity transmitted, I_0 is the incident beam intensity, μ is the linear absorption coefficient of the material for X-rays and x is the thickness of the absorbing layer. In other respects, for texture analysis in cylindrical samples, this proportion must be calculated considering the sample orientation with regard to the radiation one, and considering the θ, ψ and ϕ values. A similar model used to calculate the geometric factor $G(\psi,\theta)$ was employed [8]. For every ray of the beam, the analysis is performed assuming that the sample element around the impact point is plane and perpendicular to the normal in this point. The ray tracing Monte-Carlo method was applied to obtain the penetration depth for a known fraction of the incident beam, taking into account the orientation (ψ, ϕ) and a great number of rays. As an example, Fig. 2 shows the variation of the penetration depth as a function of tilt angle $\psi(\phi = 0)$ when the diffracted beam is ten times lower than the incident beam. From this figure, it can be seen that in the best case (i.e., for $\psi = 0$) 90% of the incident beam is absorbed at 3.9-μm depth. This result is in agreement with the experimental observations as indicated above.

The ODF calculation allowed one to obtain the texture index J. This rating corresponds to the ODF squared coefficients sum divided by $2L + 1$ ($J = 1$ for an isotropic sample). Texture being described in a three-dimensional space, it is difficult to achieve comparisons using only the J factor as a basic parameter. Nevertheless it indicates a rough trend of the material crystalline anisotropy. The J factors obtained for the studied samples are presented in Fig. 3. We point out an important variation of this index within the very first micrometers from the surface of the tube, the finished tube being the more strongly affected.

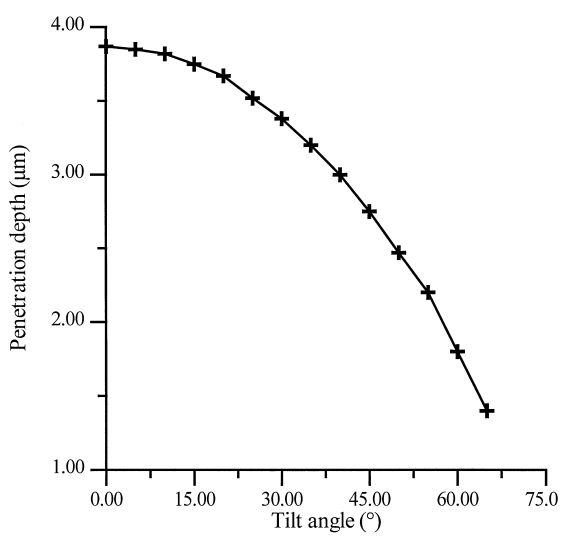

Fig. 2. Penetration depth for 90% of X-ray beam in ZY4 for a copper K_α radiation as a function of the ψ tilt angle and for $\phi = 0$ in a cylindrical sample.

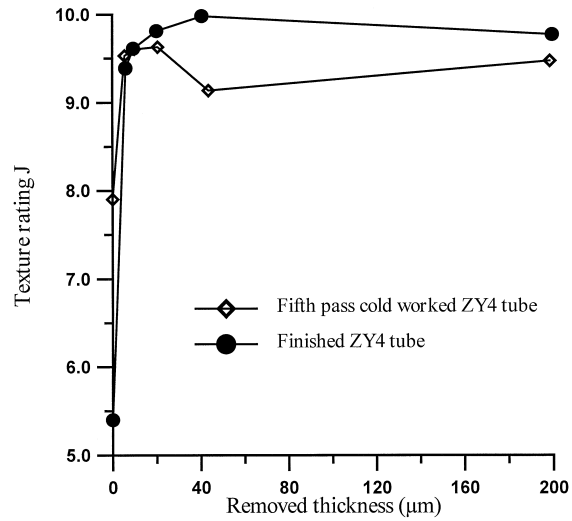

Fig. 3. Variation of texture rating J in ZY4 tubes as a function of removed thickness for fifth pass cold worked (CW series) and finished (F series) samples.

It must be noticed that experimental PF (00.2) obtained on tubes are not exactly the same than those measured on unrolled samples. The asymmetry observed in ND–RD plane, due to the cold-pilgering process, is more pronounced in unrolled tubes. The applied corrections for tubes tend to exaggerate the intensity in the central part of PF. Nevertheless, ODF analysis allows to smooth differences and to find similar recalculated PF.

3.2. Residual-stress analysis

In order to take into account the stress redistribution in the thickness of the tube that occurs during the layer removal, we performed an incremental correction following Moore and Evans' work [12].

The tangential (hoop) residual-stress analysis has been achieved using the (10.4) reflection and putting the sample perpendicularly to the diffraction plane. The results are presented in Fig. 4. These curves show that the surface stresses are compressive for both the CW and the finished tube. For the CW tube, stresses vary from -116 MPa for the CW0 sample to $+12$ MPa for the CW5 sample staying nearly constant in the depth of the tube. Besides, the finished tube has a -232 MPa compressive stress at the surface for the F0 sample and reaches very weak stress values only for the sample F41 ($+3$ MPa). Stress values at 200 μm depth show that the stress seems to be homogeneous inside the tube for both CW and F tubes. The stress in CW tubes surface results from the cold-pilgering process which imposes a combination of advance and rotation

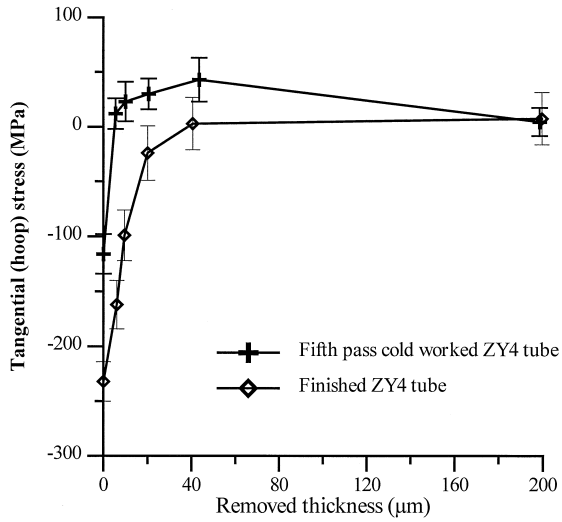

Fig. 4. Tangential (hoop) stress of ZY4 tubes as a function of removed thickness for fifth pass cold worked (CW series) and finished (F series) samples, obtained from XRD strain measurements in (104) plane.

of the tube with significant friction between tool and the surface. For the fifth pass, a material element goes through a series of about one hundred strokes during its motion from entry to exit of the mandrel. Every stroke produces such a small equivalent strain ($\Delta\varepsilon \sim 0.02$ to 0.03) that it can be assumed that the final strain is axi-symmetrical. This phenomenon concerns only the first micrometers of surface layers. The stress in the finished tubes may be attributed to the burnishing and the related depth (between 20 and 40 μm) is in agreement with general results obtained for this kind of mechanical process.

The axial stresses analysis has been achieved by putting the tube axis parallel to the diffraction plane. The results obtained on the CW tube using (10.4) and (20.2) reflections are presented in Fig. 5. As for the previous results, there is a stress variation between the non-removed tube and the others. Moreover, the stress signs obtained for the two planes are opposite. Actually, the stresses calculated for the (10.4) line vary between −16 MPa (CW0, nonremoved) and +168 MPa (CW20, 20 μm removed). On the other hand, stresses calculated for the (20.2) line vary between −312 MPa (CW0) and −193 MPa (CW20). This difference of sign has already been pointed out for residual stresses on ZY4 [13]. As a matter of fact, it has been shown [14] that the strain measured by X-ray diffraction depends not only on the macroscopic stress σ^{I} but also on the pseudo macrostrain $\varepsilon^{\mathrm{II}}_{\phi\psi}$:

$$\varepsilon_{\phi\psi}\{hkl\} = F_{\phi\psi}\{hkl\}\sigma^{\mathrm{I}} + \varepsilon^{\mathrm{II}}_{\varphi\psi}\{hkl\} \quad (2)$$

with $F\phi\psi\{hkl\}$ the X-ray elasticity constants and $\varepsilon^{\mathrm{II}}_{\phi\psi}$ the mean value of strain incompatibilities between the diffracting and the nondiffracting volumes. The second term in Eq. (2) could be associated to a 'measured' stress as

$$F_{\phi\psi}..\sigma_{\mathrm{meas}} = F_{\phi\psi}..\sigma^{\mathrm{I}} + \varepsilon^{\mathrm{II}}_{\phi\psi}\{hkl\} \quad (3)$$

so:

$$\sigma_{\mathrm{meas}} = \sigma^{\mathrm{I}} + \left(F^{t}_{\phi\psi}F_{\phi\psi}\right)^{-1}F^{t}_{\phi\psi}\varepsilon^{\mathrm{II}}_{\phi\psi}\{hkl\} \quad (4)$$

and

$$\sigma_{\mathrm{meas}} = \sigma^{\mathrm{I}} + \sigma^{\mathrm{pm}}\{hkl\} \quad (5)$$

with $\sigma^{\mathrm{pm}} = (F^{t}_{\phi\psi}F_{\phi\psi})^{-1}F^{t}_{\phi\psi}\varepsilon^{\mathrm{II}}_{\phi\psi}\{hkl\}$.

As can be seen from Eq. (5), the measured stress depends on macrostress σ^{I} and on a pseudo-macrostress σ^{pm}, function of $\{hkl\}$ planes. Besides, because of the texture, most of the (10.4) planes have the $\vec{c}$ axis making an angle between 0° and 30° with the sample surface when this axis is located preferentially between 30° and 60° in

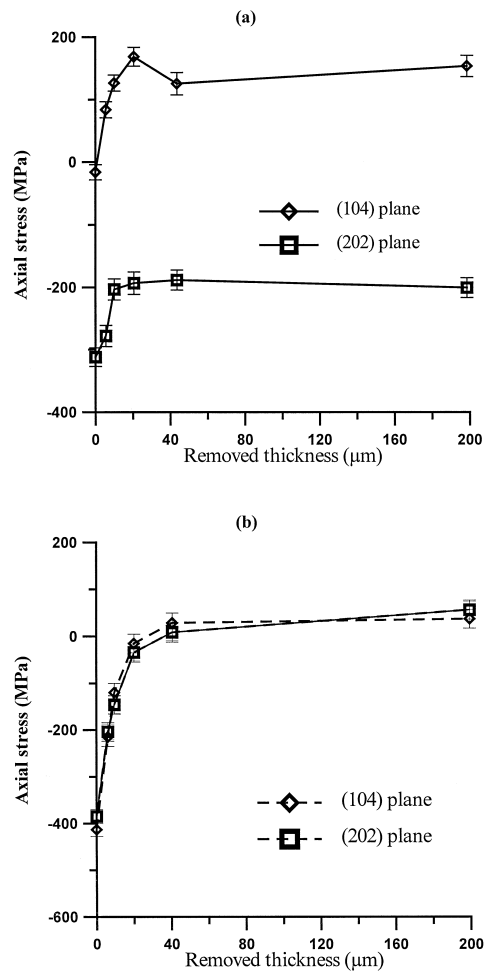

Fig. 5. Axial stress of ZY4 tubes, as a function of removed thickness, obtained from XRD strain measurements in (104) and (202) planes for (a) fifth pass cold worked (CW series) and (b) finished (F series) samples.

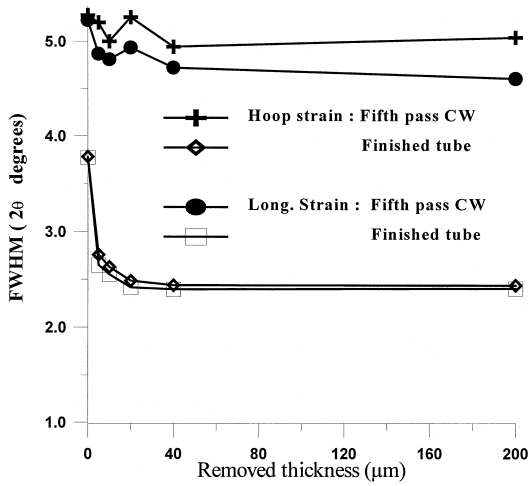

Fig. 6. Mean values of full width at half maximum (FWHM) obtained from X-ray diffraction peaks analysis as a function of removed thickness in ZY4 tubes.

relation to the surface for the (20.2) planes. The diffracting crystals are not the same for each case, which allows us to deduce that different second-order stresses exist, linked to a strong anisotropic plastic deformation for these two plane families.

From our results, it can be confirmed that, for cold-worked tubes, cold pilgering produces mainly axial residual stresses. Because of second-order stresses, the obtained values are not directly related to those obtained by macroscopic methods [15].

The axial stresses of the finished tubes are shown in Fig. 5b. This time, the stresses variation in relation to the thickness does not depend on the considered reflection. For both reflections (10.4) and (20.2), the stress is quite important, about −410 MPa, on the F0 sample and −385 MPa for the CW0 sample. This stress decreases down to zero with layer removal. The thermal treatment achieved on the finished tube seems to have relaxed the second-order stresses noticed for the CW tubes which is consistent with the fact that burnishing does not produce strong plastic flow. Moreover, the strong compressive stress observed on the non removed tube is probably due to the finishing burnishing because the thickness affected by this treatment is quite the same as the thickness observed for the tangential stresses. Stronger values for axial stress than for tangential one in (10.4) planes may be attributed also to the online directional burnishing process.

The Full Width at Half Maximum (FWHM) of X-ray diffraction peak allows us to obtain information about the size and the distortion of coherently diffracting domains induced, for instance, by work hardening. For CW tubes, the FWHM is quite important (5°) and homogeneous in the analysed depth (see Fig. 6). This value is in agreement with the high strain rate imposed by the cold pilgering. The lower values of FWHM for the finished tube compared with the CW tube show that heat treatment has strongly reduced the effects of work hardening. Besides, for the F0 tube, the FWHM value (3.7°) is higher than the other finished tubes, confirming the burnishing effects. This behaviour seems to concern only the first micrometers as it can be seen from Fig. 6, in agreement with the texture index J behaviour. In the case of the longitudinal stress, the variation of FWHM is rather the same than that observed in tangential stress study.

Taking into account that second and third order stresses affect X-ray diffraction profile peaks, advanced profile analysis will be done to identify instrumental and structural factors involving observed diffraction peaks broadening.

4. Conclusion

X-ray diffraction texture analysis on Zircaloy-4 tubes has shown asymmetric (00.2) pole figure for the finished tube surface. This asymmetry was not observed on unrolled tubes. X-ray diffraction stress analysis in axial direction showed second order stresses for cold-worked tubes which seem to have been relaxed by thermal treatments.

References

[1] D.O. Hobson, P.L. Rittenhouse, Trans. Met. Soc. AIME 245 (1969) 797.
[2] E. Tenckhoff, ASTM STP 754 (1982) 5.
[3] N. Nagai, T. Kakuma, K. Fujita, ASTM STP 754 (1982) 26.
[4] L. Brunisholz, C. Lemaignan, ASTM STP 939 (1987) 700.
[5] S.R. Mac Ewen, C.N. Tomé, J. Faber, Acta Met. 37 (1989) 979.
[6] R. Guillén, J.L. Féron, J.L. Glimois, F. Hunt, J. Le Pape, J. Sénevat, Textures Microstruct. 14–18 (1991) 519.
[7] J.L. Bardon, C. Esling, J.L. Féron, D. Gex, J.L. Glimois, R. Guillén, M. Humbert, P. Lemoine, J. Le Pape, J.P. Mardon, A. Thil, G. Uny, Textures Microstruct. 2 (1989) 1.
[8] R. Guillén, C. Cossu, T. Jacquot, M. François, B. Bourniquel, submitted to J. Appl. Crystallogr.
[9] R. Guillén, M. François, B. Bourniquel, E. Girard, to be submitted.
[10] L. Wcislak, H.L. Bunge, Texture Microstruct. 14–18 (1991) 257–271.
[11] B. Bourniquel, J.-L. Féron, Proc. of the Colloque du Groupement Français pour l'Analyse des Contraintes par Diffractométrie, Toulon, France, May 6–7, 1993.
[12] M.G. Moore, W.P. Evans, SAE Trans. 66 (1958) 340.
[13] E. Girard, J. Sénevat, B. Bourniquel, in: Proc. 9th Int. Symp. Progress in Metals and New Materials, Investigation Methods, Measurements of Residual Stresses, ENS des Mines de Saint-Etienne, Vol. 16, 1993, p. 26.1.
[14] J.M. Sprauel, L. Castex, EPDIC 1, Materials Science Forum, TransTech, Munich, Vols. 79–82, 1991, 143.
[15] E. Girard, doctoral thesis, University of Nantes, 1993.